UDK 665.71
Original scientific article/Izvirni znanstveni članek

ISSN 1580-2949
MTAEC9, 57(3)291(2023)

EFFECTS OF ALLOYING ELEMENTS AND SURFACE PROPERTIES ON THE CORROSION BEHAVIOR OF HVOF-DEPOSITED WC COATINGS

VPLIV ZLITINSKIH ELEMENTOV IN LASTNOSTI POVRŠINE NA KOROZIJO PREVLEK WC IZDELANIH S POSTOPKOM HVOF

Erhan Ozkan*
Dikkan R&D Center Izmir, Turkey

Prejem rokopisa – received: 2023-03-22; sprejem za objavo – accepted for publication: 2023-05-02

doi:10.17222/mit.2023.833

The main purpose of this study is to investigate the corrosion behavior of nickel-aluminum buffer and tungsten-carbide-based ceramic-metal composite coated materials on EN 1.4404 quality stainless steels in a sulfuric acid (H_2SO_4) environment for petrochemical industry applications. For this purpose, tungsten-carbide-based coatings were produced on nickel-aluminum-deposited 1.4404 stainless-steel substrates using the HVOF (High Velocity Oxy-Fuel) technique. In the characterization of coatings, X-ray diffraction (XRD) for phase analysis, optical microscope and scanning electron microscope (SEM) for surface morphology, image analyzer for coating thickness measurements, energy distribution spectroscopy (EDS) for elemental analysis, and roughness device for surface structures, were used. WC-, Co-, Ni-, and NiAl-based phases were observed in the coatings. According to metallographic studies, all the coatings had a similar coating microstructure and made good contact with the substrate. Potentiodynamic polarization measurements and corrosion tests were carried out to determine the corrosion behavior of HVOF plasma-sprayed coatings using a potentiostat/galvanostat. The results showed that the WCCo-NiAl-coated stainless-steel substrate had a higher corrosion resistance to the H_2SO_4 environment than the NiAl and WCNi-NiAl samples.

Keywords: HVOF, stainless steel, coatings, corrosion

Namen študije je bil raziskati korozijsko obnašanje z Ni-Al blažilcem in s kompozitnim keramičnim materialom na osnovi volfram karbida (WC) oplaščenim nerjavnim jeklom EN 1.4404 v okolju žveplene kisline (H2SO4), namenjenih aplikacijam v petrokemijski industriji. V ta namen so izdelali prevleke na osnovi WC na z Ni-Al prevlečenem nerjavnem jeklu vrste 1.4404 s postopkom naprševanja z visoko hitrostjo v mešanici goriva in kisika (HVOF; angl.: High Velocity Oxy-Fuel). Po izdelavi vzorcev s prevlekami so le-te ocenili. Z rentgensko difrakcijo (XRD) so izvedli fazne analize, z optičnim in elektronskim presevnim mikroskopom (SEM) so analizirali morfologijo površine prevlek, z digitalnim analizatorjem pa so določili debeline in hrapavost prevlek. Z energijsko disperzijsko spektroskopijo (EDS) so določili porazdelitev posameznih kemijskih elementov (faz na osnovi WC, Co, Ni in NiAl) na površini prevlek. Metalografske analize so pokazale, da imajo vse izdelane prevleke podobne mikrostrukture in dober stik s podlago. S pomočjo Potenciostata-Galvanostata so izvedli meritve potenciodinamične polarizacije ter korozijske teste in določili korozijsko obnašanje izdelanih plazemsko naprešenih prevlek HVOF. Rezultati raziskav so pokazali, da imajo vzorci nerjavnega jekla prevlečeni z WCCo-NiAl boljšo odpornost proti koroziji v okolju H_2SO_4 kot prevleke na osnovi NiAl in WCNi-NiAl.

Ključne besede: postopek naprševanja z visoko hitrostjo v mešanici goriva in kisika (HVOF), nerjavno jeklo, prevleke, korozija

1 INTRODUCTION

Petrochemical plants are installations for chemical conversion processes. In these facilities, chemical raw materials are produced using physical or chemical conversion processes of inorganic or organic chemicals. [1–3] The most common of these raw materials is sulfuric acid (H_2SO_4). H_2SO_4 is produced from SO_2 that is derived from a variety of sources, such as the combustion of elemental sulfur or the heating of metal sulfides. SO_2 is then converted to SO_3 using a catalyst in the gas phase chemical equilibrium reaction and reacts with water to form H_2SO_4.[4–7]

Recycling facilities have a critical structure in terms of actively positioning sustainable environmental enterprises, which are today's important facilities, in the organization.[8] H_2SO_4 formed as a result of the above chemical reactions creates an aggressive, corrosive environment in the main lines of petrochemical industries and especially in sulfuric acid recovery plants. In the petrochemical industry, surface modifications of metals have come to the fore to protect metallic surfaces from corrosion. The corrosion resistance of materials can be increased by changing and improving the surface morphology and microstructure. Changing the surface chemistry of materials is possible by carburizing, nitriding, carbonitriding, boriding, siliconization and chroming. In addition, surface-coating processes with thermal spraying have recently played a role in increasing the corrosion resistance of metallic surfaces to slow the corrosion rate and make the surface corrosion resistance more effective.[9,10]

Thermal spray processes were made with spray guns to protect the main material surface from environmental

*Corresponding author's e-mail:
erhan.ozkan@dikkan.com (Erhan Ozkan)

conditions, and to prevent corrosion by improving the material surface properties.[11–13] After the coating material is melted with the energy used in the gun, it is thrown onto the material surface at high speed and the coating is created. In particular, coatings produced with HVOF (High Velocity Oxy-Fuel) show very good adhesion and cohesion properties, as well as being very hard, making this method more advantageous than other methods.[14,15] However, the formation of holes, pores and micro-cracks as a result of high-temperature particles hitting the substrate surface at high speed can be counted among the disadvantages of this method.[16] These pores, cracks and holes have a negative effect on the corrosion behavior of the material. In order to prevent this, systems have been developed by creating a buffer layer on the coatings. Buffer layers provide great advantages in preventing formations such as capillary cracks and porosity, which reduce the corrosion resistance.[17–24]

EN 1.4402 quality stainless steel (commonly known as 316L in AISI norm) is a low-carbon stainless steel that is widely used in aggressive conditions such as sulfuric acid, thanks to its chemical content. The weak side of this stainless steel is that it cannot perform adequately in environments with more aggressive corrosion, and erosive environments. Surface coatings are applied to improve this weakness and increase the service life.

In this study the corrosion behavior of EN 1.4402 stainless steels, which are widely used in the petrochemical industry, coated with NiAl, WC-Co and WC-Ni by HVOF technique was evaluated in a 1-N H_2SO_4 solution with potentiodynamic methods. According to the results obtained, the data on the prolongation of the service life of surfaces with different alloy values were transferred in detail, and technological solution methods were proposed by disseminating the results. In addition, HVOF coating parameters, porosities of coating surfaces, surface thicknesses, microstructures, and their interactions and changes with the corrosion behavior of the coatings were presented to provide additional information.

2 EXPERIMENTAL PART

EN 1.4402 stainless-steel samples with the dimensions of (50 × 50 × 2) mm were used as a substrate material. The surface preparation of the parts used in the HVOF technique is an important step. This is because the structure of the coatings spreads directly with the surface roughness and is controlled by the type of blast, pressure, angle, width, duration and sand-blast nozzle (hole size). The material surface was sandblasted prior to the HVOF thermal spraying for the purpose of maintaining the strength durability of the coating. Aluminas at high outputs were impacted on the material at high speeds, increasing the roughness of the surface and notes the number and size of surface asperities with increasing roughness. During the spraying process, it attached itself to this surface mechanically and physically by clinging to these asperities coming from the earth. A high bond strength could only be achieved with the expected high roughness, and this caused incresing resistance of the coating powders to withstand the substrate values. This process was carried out with 35-grit alumina powders for 30 s using 400-kPa air. Then, via Metco Diamond Jet (DJ) 2600 brand system, a coating was obtained with traditional sintered powders having a grain size of 14 μm in the ratio of 13 *w*/% Co, 87 *w*/% WC and 13 *w*/% Ni and 87 *w*/% WC, but the cracks on the surfaces of the obtained coatings had a negative effect on the wear. An interlayer coating containing nickel and aluminum was carried out to ensure the resistance of the WC-based cermet coatings to the substrate. To limit the content of the intermediate layer, the bond from the literature and previous properties was used and accordingly NiAl containing 95 *w*/% Ni, 5 *w*/% Al was used as the powder coating. The NiAl coating and WC basis, bond parameters of the two coatings are given in **Table 1**.[24]

Table 1: HVOF coating process parameters

Parameters	Values	
	NiAl	WC-based coatings
Rate of oxygen flow (L min^{-1})	135	245
Rate of hydrogen as fuel gas (L min^{-1})	410	650
Rate of nitrogen as carrier gas (L min^{-1})	20	18
Distance of spray (mm)	260	310
Velocity of horizontal substrate (m s^{-1})	1	1
Speed of traverse vertical gun (mm s^{-1})	5	5
Layer number	30	30

A Rigaku D/Max-2200/PC Model diffractometer was used for the X-ray diffraction (XRD) of the as-sprayed coatings using Cu-K_α radiation (0.15406 nm), a 0.05° step size, and a 2-s dwell duration to confirm the crystallinity of the coatings. The coatings were cold molded in the way of using the cross-sectional areas of the samples for optical microscope examinations. In order to obtain better optical microscope results, specimens were grinded and polished to a 0.1-μm finish surface. Using a spark wire cutter, coating cross-sections were separated from the batch. A Nikon Eclipse LV 150 optical microscope and a LUCIA 4.21 image analyzer were used for the measurement of the coating thickness. The surface morphology of the coatings was investigated with a JEOL JJM 6060 scanning electron microscope (SEM) coupled with energy-dispersive spectroscopy (EDS). Surface-roughness measurements were performed with a Mitutoyo SJ-301 surface-roughness tester.

The corrosion behavior of the coatings was evaluated using a standard potentiodynamic polarization technique with a GAMRY PC4/750 Potentiostat/Galvanostat Model. The NiAl-, WCNi-NiAl- and WCCo-NiAl-coated EN 1.4402 stainless-steel samples were ultrasoni-

cally cleaned in acetone for 15 min before the experiments. Prior to the corrosion tests, uncoated parts of the substrate were lacked with polimeric materials to only have a coating surface. The electrochemical system consisted of a corrosion cell, a potensiostat/galvonostat and a computer. The corrosion cell used was GAMRY's newly designed cell. The reference electrode used in this study was a saturated calomel electrode (SCE). The working solution was selected as 1-N H_2SO_4 due to the petrochemical industry applications. The tests were conducted at room temperature, which varied from 24 °C to 27 °C. During this time, the corrosion potential of the samples was also monitored. Potential scans for the polarization were initiated at –500 mV and end at 4000 mV. A constant potential scan rate of 5 mV s^{-1} was used. To observe the characteristics of the corrosion test, the differences in the pre- and post-corrosion surface images of the samples and the changes in coating thickness and surface roughness were observed. The electrochemical method was used the observe the amount of porosity for the HVOF-coated specimens.

3 RESULTS

Figure 1 illustrates XRD patterns of NiAl pre-coated and WC with Co and WC with Ni coatings deposited by HVOF technique on 1.4402 SS substrates. According to XRD results, different forms of tungsten carbide and its derivatives, tungsten carbide cobalt alloys and nickel aluminum were determined.

Even though WC, W_2C, W, and FeNi phases were found with the WCNi-NiAl coatings, WC, W_2C, W, and Co phases were determined from the WCCo-NiAl-coated stainless steel substrate. W_2C and metallic W phases, which were obtained in both WC-based layers after deposition process, were formed by carbon losses during the coating step. A NiAl phase was found from both of the samples because of the NiAl bond layer on the substrate. However, it is important to express that the electrochemical corrosion behaviours of the WCCo-NiAl and WCNi-NiAl layers are complex because these coatings consist of different phases.

SEM was used for the larger-scale microstructure analysis. **Figure 2** demonstrates surface morphologies of

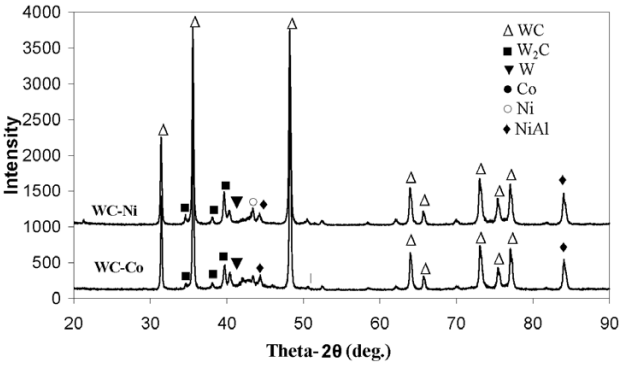

Figure 1: XRD patterns of the HVOF-coated NiAl, WC, WCCo, WCNi specimens

the NiAl, WCCo and WCNi coatings produced using the HVOF system. It was determined that the coatings usually exhibit porosity, microcracks and unmelted particles according to the SEM evaluations. As reported in [23], SEM images showed that the bond between the substrate and the coating was strong, due to the dense layer of the coating. Due to the application principles of the HVOF process, incompletely melted particles caused plastic damage on the surface, causing micro-cracks and pores in general.

The weakness of he HVOF-sprayed coatings, i.e., pores, microcracks and unmelted particles, are the areas that activate corrosion, especially in H_2SO_4 solutions. Even if these inhomogeneties are very small structures, unfortunately some of them are interconnected in these coatings, allowing penetration of the coating by a fluid. Additionally, since this technique has these kinds of advantages compared to other thermal spray techniques, such as electric arc, flame spray, plasma spray and detonation gun, WC-based HVOF-sprayed coatings have become important in petrochemical applications. The other significant issue here is the surface morphology of the coatings for corrosion behaviours. Upon investigating the surface morphologies, the WCCo coating has similar features to WCNi, but NiAl possess distinctly different microstructures. The NiAl metallic coatings have very large splats with microcracks, compared to the WC-based coatings. The splat sizes of the NiAl, WCCo

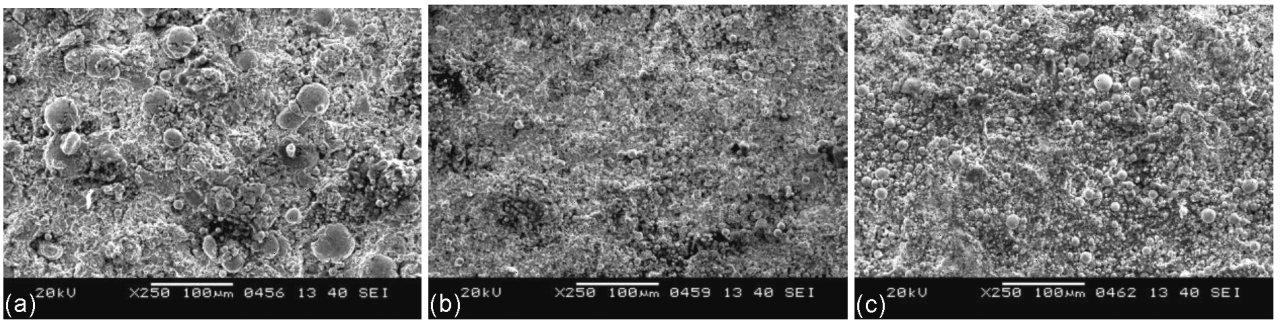

Figure 2: Surface morphologies of: a) NiAl, b) WCCo-NiAl and c) WCNi-NiAl layers produced by HVOF system prior to corrosion tests. The scale bars of all coatings are 100 μm.

Table 2: Electrochemical measurements of the coatings in 1-N H_2SO_4 solution at 25 °C

Samples	E_c (mV vs SCE)	β_c (mV)	β_a (mV)	I_{cor} (A)	Pol. Res. (R) (Ω)	Porosity (%)
NiAl	–340	309,4	312,3	459×10^{-6}	1.90×10^5	8.24
WCCo-NiAl	–250	375,0	283,9	727×10^{-7}	9.66×10^5	5.58
WCNi-NiAl	–300	207,9	172,6	929×10^{-6}	3.18×10^5	7.60

and WCNi coatings are approximately (50, 10 and 15) μm, respectively.

From the aspect of corrosion, the porosity, surface roughness, coating thickness, bond layer, pinhole and microcrack are significant issues for HVOF-sprayed coatings. The coating itself may be very resistant to corrosion, but if the corrosion media can penetrate to the substrate from the microstructural defects in the coatings, the corrosion resistance of the substrate also becomes important. The cathodic and anodic electrochemical behaviors of the NiAl-, WCCo-NiAl-, and WCNi-NiAl-coated stainless-steel samples were investigated in 1-N H_2SO_4 solutions. The electrochemical measurements of the NiAl-, WCCo-NiAl-, WCNi-NiAl-coated stainless-steel samples and the bare substrate are presented in **Table 2**.

The porosities of the coatings were calculated using electrochemical methods and the following equation.[25]

$$F = \frac{R_{p,m}}{R_p} \log\left(-\frac{|\Delta E_{cor}|}{\beta_a}\right) \quad (1)$$

In this equation F represents the total coating porosity, $R_{p,m}$ is the polarization resistance of the base material, R_p is the measured polarization resistance of the coated samples, ΔE_{cor} is the difference between the corrosion potentials of the surfaces with and without the coating, and β_a is the anodic Tafel slope of the base material.

The anodic polarization behaviours of the layers on the stainless steel are given in **Figure 3**. The corrosion potentials of the NiAl, WCCo-NiAl, WCNi-NiAl coatings are (–340, –250, and –300) mV, respectively. Moreover, the corrosion current values of the NiAl, WCCo-NiAl, and WCNi-NiAl coatings were (459×10^{-6}, 727×10^{-7} and 929×10^{-6}) A, respectively. The WCCo-NiAl layered sample was the most stable coating with respect to the H_2SO_4 corrosive environment due to the passive-film-forming effect of Co and its low potential.

As shown in **Figure 3**, the curves for the WCCo-NiAl and WCNi-NiAl samples can be divided into two areas. In the first field where the potential value is lower than 1 V, the current values increase exponentialy with the increasing potential. Despite the fact that the first field behavior resembles a passive layer, which differs from the overall passive behavior. The current field I is observed for currents above about 100 mA. This is high compared to the typical passive current of about 10 mA. This also means that alloying has a great influence on the coating layer's anodic reaction. Region I was formed as a result of IR degradation due to surface corrosion products' deposition of the layer combined with the binder material's dissolution. For the WCCo-NiAl deposit, region I is formed by Co and W oxidation. Interestingly, the NiAl coating exhibited a general passivation behavior similar to the stainless-steel samples containing active, passive and transpassive regions.

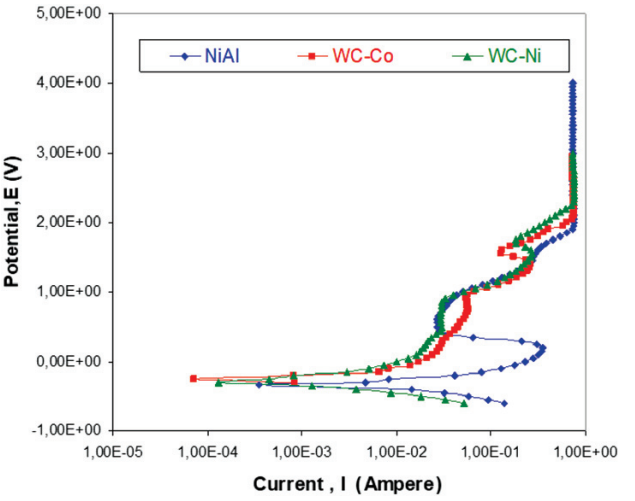

Figure 3: Anodic polarization curves of NiAl, WCCo-NiAl and WCNi-NiAl coatings

Figure 4 shows SEM micrographs taken from the surfaces of the NiAl, WCCo-NiAl and WCNi-NiAl coatings after the corrosion tests. A few holes and pits were observed on the surfaces of all the coatings. Notably, an examination of the corroded samples revealed localized corrosion spots on the surface. In addition to these, before the corrosion tests, cross-sectional optical microstructural observations included many scratches and it was difficult to separate the coating and base material with the naked eye. On the other hand, after the corrosion tests, separation became easier, the coating appeared, and the scratches removed owing to the acidic conditions. Therefore, it can be said that the corrosion tests acted as an electro-polishing process, which caused to the coatings to be seen more clearly and formed unscratched structure. SEM micrographs of the coatings strongly supported the anodic polarization results. Although several holes and pits were observed on the surfaces of the NiAl and WC-Ni coatings, uniform corrosion was found for the WCCo coating. As mentioned before, a H_2SO_4 solution was our corrosive environment used in the experiments. On the other hand, S and O

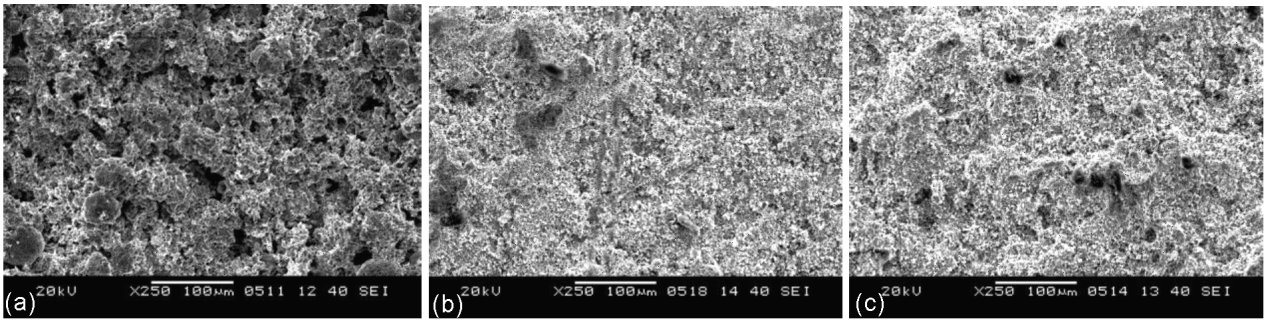

Figure 4: Surface morphologies of: a) NiAl, b) WCCo-NiAl and c) WCNi-NiAl coatings after electrochemical corrosion tests. The scale bars of all coatings are 100 µm

were the most effective elements for the corrosion reactions in this acidic environment.

The SEM micrographs of the coating layers and the maps for the sulphur and oxygen as corrosion products are depicted in **Figure 5**. It is possible to see from this figure that the S and O distributions are the most dense and regular in the NiAl coating (see **Figure 5a**). The S and O are rarely and irregularly distributed in the WCNi and WCCo coatings (see **Figure 5b** and **5c**).

In the corrosion of the coatings, there were a lot of parameters influencing the corrosion behaviours. These parameters were coating structures such as porosity, surface roughness, and thickness. The porosity values of the coatings are listed in **Table 2** and the porosity percentages of the NiAl, WCCo and WCNi coatings were determined to be 8.24, 5.58 and 7.60, respectively. The NiAl coatings possessed the highest porosity content. During the corrosion tests, the porosities became potential zones

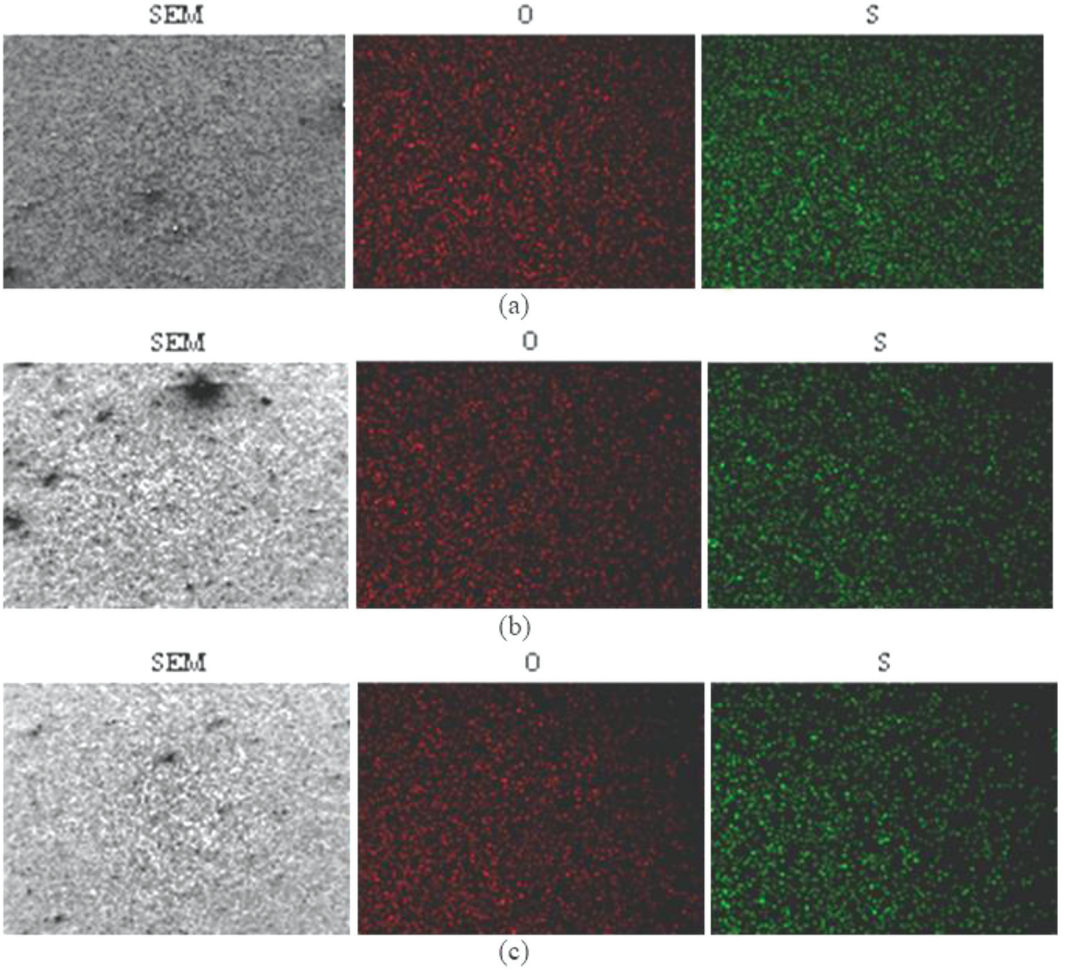

Figure 5: The SEM micrographs of the coatings and X-ray maps of sulphur and oxygen elements as corrosion products The SEM micrographs of the coatings and X-ray maps of sulphur and oxygen elements as corrosion products after electrochemical corrosion tests. The corroded samples are: a) NiAl, b) WCCo-NiAl and (c) WCNi-NiAl coatings.

to the corrosive environment and reacted first. Because of this the corrosion resistance of the coatings decreased with increasing porosity.

The changes in the coatings' surface roughness before and after the corrosion tests are presented in **Table 3**. The surface structure of the coatings before the corrosion tests was relataed to the HVOF process parameters. The particle distribution, shape, size and parameters of the atomization could form open porosities, causing accelerated corrosion speed on the surface of the coatings. Additionally, the surface-roughness values (R_a) are important to determine some corrosion phenomena. The R_a values of the coatings increased after the corrosion tests, except the sample with the WCCo layer. The reason for this phenomenon was the amount of porosity that the coating contains. Also, the polarization resistance can be explained as a function of the surface roughness. Polarization means a deviation from the ideal situation. Polarization resistance is the prevention of the polarization of the materials. Surface roughness is an important parameter on the polarization resistance of the coatings. The general rule is an increase of the surface roughness casuses a decrease of the polarization resistance.

Table 3: Surface roughness of the coatings before and after corrosion tests

Coatings	Before Corrosion Tests			After Corrosion Tests		
	R_a	R_z	R_q	R_a	R_z	R_q
NiAl	8.61	57.59	10.77	8.63	58.77	11.29
WCCo-NiAl	7.73	45.04	9.41	6.17	48.82	8.42
WCNi-NiAl	8.01	48.08	9.71	8.05	52.43	10.22

Figure 6 shows the change in polarization resistances of the surface roughness for the NiAl-, WCCo-NiAl-, and WCNi-NiAl-coated samples. It is clear from the figure that the resistance of the corrosion decreased with increasing surface roughness for the different coatings. That is to say, surface roughness is one of the important parameters to determine the polarization resistance of the coatings.

The coating thicknesses before and after the corrosion tests are given in **Table 4**.

Table 4: Change in coating thickness

Samples	Before Corrosion Tests	After Corrosion Tests
NiAl	719 μm	626 μm
WCCo-NiAl	514 μm	507 μm
WCNi-NiAl	513 μm	471 μm

Figure 7 denotes a decrease of the coating thickness depending on the corrosion time, which took 167 min because the scan rate was constant (5 mV s^{-1}). The thicknesses of the NiAl, WCCo-NiAl and WCNi-NiAl layers were measured to be (719, 514 and 513) μm before the corrosion tests, respectively. These thickness values of the NiAl, WC–Co/NiAl and WC–Ni/NiAl coatings decreased to (626, 507 and 471) μm after the corrosion tests, respectively. Therefore, the WCNi coatings had the highest corrosion rate. This is an expected result, because the WCNi coating has the highest negative corrosion potential.

4 DISCUSSION

The corrosion behaviors of the HVOF sprayed NiAl, WCCo-NiAl and WCNi-NiAl coatings on EN 1.4402 substrates were investigated for petrochemical industries. The obtained resultes are summarized as follows;

The WCCo and WCNi coatings without buffere exhibited porosity, microcracks and unmelted particles according to SEM evaluations. Even if these inhomogeneties were small structures, some of them are interconnected in these coatings, allowing penetration of the coating by a fluid. Therefore, a NiAl buffer layer was

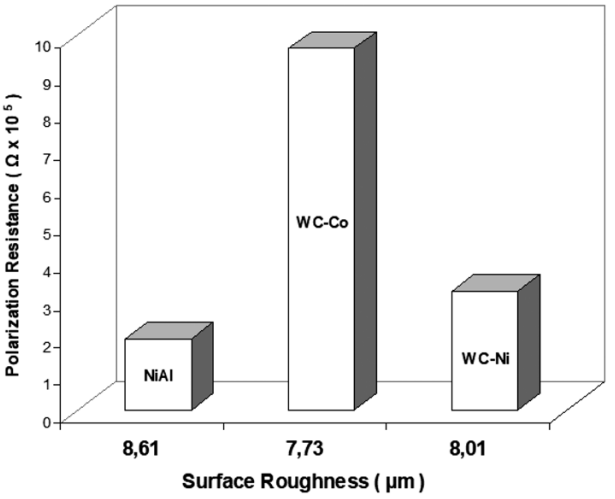

Figure 6: Polarization resistance versus surface roughness for the coatings

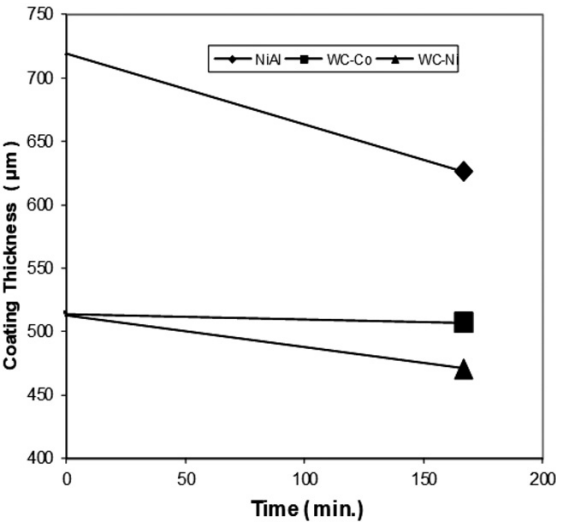

Figure 7: Change in coating thickness versus time

applied to the coatings and no cracks were observed on the surfaces.

W, C, WC, W_2C, and NiAl phases were detected as common in WCCo and WCNi coatings. The NiAl phase originated from the buffer layer, while the W, C, W_2C phases originated from the carbide coating HVOF process.

The corrosion potentials of the NiAl, WCCo-NiAl, WCNi-NiAl coatings are -340, -250, and -300 mV, respectively. Of these materials, the WCCo-NiAl layered sample is the most stable coating with respect to the H_2SO_4 corrosive environment. After the corrosion tests, a number of holes and pits were observed from the surfaces of all the coatings. The S and O distribution is the most dense and regular in the NiAl coating. The S and O are rarely and irregularly distributed in the WCNi and WCCo coatings.

Porosity was measured by using the electrochemical technique. Depending on this, the porosity percentages of NiAl, WCCo and WCNi coatings were determined to be 8.24, 5.58 and 7.6, respectively.

An increase of the surface roughness casused a decreasing polarization resistance. The corrosion resistance decreased with an increasing surface roughness for the different coatings.

The thicknesses of the NiAl, WCCo-NiAl and WCNi-NiAl layers were measured to be 719, 514 and 513 μm before the corrosion tests, respectively. These thickness values of NiAl, WCCo-NiAl and WCNi-NiAl coatings decreased to (626, 507 and 471) μm after the corrosion tests, respectively.

5 CONCLUSIONS

The results showed that the WCCo-NiAl-coated stainless-steel substrate had a higher corrosion resistance to the H_2SO_4 environment than the NiAl and WCNi-NiAl samples. While the close densities of the cobalt and nickel did not allow a realistic comparison of the process, it was observed that cobalt had smaller particles in the HVOF process due to its slightly higher melting point. This resulted in a lower porosity rate in the coating. Moreover, increasing the porosity caused an increasing corrosion rate. Therefore, the WCNi-NiAl showed a lower corrosion resistant compared to the WCCo-NiAl coatings, despite its emf series upper position. As a result, this article will increase the gains of the sector, with the efforts to improve the erosion and corrosion behavior of EN 1.4402 stainless steels, which are widely used in the petrochemical industry, and to improve their service life.

6 REFERENCES

[1] M. K. Lauer et al., Durable cellulose–sulfur composites derived from agricultural and petrochemical waste., Advanced Sustainable Systems., 3.10 (**2019**), 1900062, doi:10.1002/adsu.201900062

[2] M. A. F. de Carvalho et al., A potential material for removal of nitrogen compounds in petroleum and petrochemical derivates., Chemical Engineering Communications., 208.11 (**2021**), 1564–1579, doi:10.1080/00986445.2020.1798938

[3] C. P. Lawagon et al., Sulfonated graphene oxide from petrochemical waste oil for efficient conversion of fructose into levulinic acid., Catalysis Today., 375 (**2021**), 197–203, doi:10.1016/j.cattod.2020.02.036

[4] M. Adimi, M. Maziar, H. Fathinejadjirandehi, Treatment of petrochemical wastewater by modified electro-fenton method with nano porous aluminum electrode., Journal of Water and Environmental Nanotechnology., 2.3 (**2017**), 186–194, doi:10.22090/jwent.2017.03.006

[5] H. Hassani, S. Emmanuel Sirimal, A. M. Al Kaabi. The role of innovation and technology in sustaining the petroleum and petrochemical industry., Technological Forecasting and Social Change., 119 (**2017**), 1–17, doi:10.1016/j.techfore.2017.03.003

[6] E. de Jong, G. Jungmeier, Biorefinery concepts in comparison to petrochemical refineries., Industrial biorefineries & white biotechnology. Elsevier., (**2015**), 3–33, doi:10.1016/B978-0-444-63453-5.00001-X

[7] R. A. Meyers, Handbook of petrochemicals production processes, McGraw-Hill Education, 2019

[8] A. I. Shinkevich et al., Key directions of automation of petrochemical production, Journal of Physics: Conference Series, IOP Publishing, 1515 (**2020**) 2

[9] T. Bondarenko et al. Investments to the petrochemical sector: the value of the competitiveness of petrochemical companies, 2020

[10] S. Wylie, N. Shapiro, M. Liboiron, Making and doing politics through grassroots scientific research on the energy and petrochemical industries., Engaging Science, Technology, and Society., 3 (**2017**), 393–425, doi:10.17351/ests2017.134

[11] Y. Jianhui et al., Improving the wear resistance of HVOF sprayed WC-Co coatings by adding submicron-sized WC particles at the splats' interfaces, Surface and Coatings Technology., 285 (**2016**), 17–23, doi:10.1016/j.surfcoat.2015.11.017

[12] W. Fu et al., Microstructure and properties of high velocity oxygen fuel sprayed (WC-Co)-Ni coatings., Ceramics International., 46.10 (**2020**), 14940–14948, doi:10.1016/j.ceramint.2020.03.021

[13] A. Rehan et al., Comparative study of corrosion performance of HVOF-sprayed coatings produced using conventional and suspension WC-Co feedstock., Journal of Thermal Spray Technology., 27 (**2018**), 1579–1593, doi:10.1007/s11666-018-0775-2

[14] Y. Liu et al., Erosion–corrosion property of CeO 2-modified HVOF WC-Co coating., Journal of Thermal Spray Technology., 25 (**2016**), 815–822, doi:10.1007/s11666-016-0391-y

[15] M. M. M. Sarcar, K. N. S. Suman, S. Kamaluddin, Tribological and corrosion behavior of HVOF sprayed WC-Co, NiCrBSi and Cr3C2-NiCr coatings and analysis using design of experiments., Materials Today: Proceedings., 2.4–5 (**2015**), 2654–2665, doi:10.1016/j.matpr.2015.07.227

[16] A. Alhaji et al., Electroless nickel–phosphorus plating on WC–Co powders using HVOF feedstock., Surface Engineering., 35.2 (**2019**), 120–127, doi:10.1080/02670844.2018.1477558

[17] P. K. Katiyar, R. Navneet Singh, Corrosion behavior of WC-Co tool bits in simulated (concrete, soil, and mine) solutions with and without chloride additions., International Journal of Refractory Metals and Hard Materials., 85 (**2019**), 105062, doi:10.1016/j.ijrmhm.2019.105062

[18] I. Hulka et al., Effect of Ti addition on microstructure and corrosion properties of laser cladded WC-Co/NiCrBSi (Ti) coatings., Applied Surface Science., 504 (**2020**), 144349, doi:10.1016/j.apsusc.2019.144349

[19] X. Zhang et al., Effects of Ni addition on mechanical properties and corrosion behaviors of coarse-grained WC-10 (Co, Ni) cemented carbides., International Journal of Refractory Metals and Hard Materials., 80 (**2019**), 123–129, doi:10.1016/j.ijrmhm.2019.01.004

[20] F. S. da Silva et al., Corrosion behavior of WC-Co coatings deposited by cold gas spray onto AA 7075-T6., Corrosion Science., 136 (**2018**), 231–243, doi:10.1016/j.corsci.2018.03.010

[21] Q. Zhang et al., Corrosion behavior of WC–Co hardmetals in the oil-in-water emulsions containing sulfate reducing Citrobacter sp., Corrosion Science., 94 (**2015**), 48–60, doi:10.1016/j.corsci.2015.01.036

[22] M. Erfanmanesh et al., Friction and wear behavior of laser cladded WC-Co and Ni/WC-Co deposits at high temperature., International Journal of Refractory Metals and Hard Materials., 81 (**2019**), 137–148, doi:10.1016/j.ijrmhm.2019.02.025

[23] A. M. F. Rocha et al., Corrosion behaviour of WC hardmetals with nickel-based binders., Corrosion Science., 147 (**2019**), 384–393, doi:10.1016/j.corsci.2018.11.015

[24] E. Celik, O. Culha, B. Uyulgan, N.F. Ak Azem, I.Ozdemir, A. Turk., Assessment of microstructural and mechanical properties of HVOF sprayed WC-based cermet coatings for a roller cylinder., Surface and Coatings Technology, (**2006**), 4320–4328

[25] B. C. Oberländer, E. Lugscheider, Comparison of properties of coatings produced by laser cladding and conventional methods., Materials Science and Technology, 8.8 (**1992**), 657–665